Received 13 February 2022; accepted 3 March 2022. Date of publication 9 March 2022; date of current version 18 March 2022.

Digital Object Identifier 10.1109/OJAP.2022.3158203

Graphene Based Tunable Terahertz Holographic Antennas

PENGFEI REN [1], LIJUN JIANG [2], AND PING LI [1] (Senior Member, IEEE)

[1]Key Laboratory of Ministry of Education of China for Research of Design and Electromagnetic Compatibility of High Speed Electronic Systems, Shanghai Jiao Tong University, Shanghai 200240, China

[2]Department of Electrical and Electronic Engineering, The University of Hong Kong, Hong Kong

CORRESPONDING AUTHOR: P. LI (e-mail: ping.li@sjtu.edu.cn)

This work was supported in part by NSFC under Grant 61831016 and Grant 62071290, and in part by the Shanghai Committee of Science and Technology under Grant 20501130500.

ABSTRACT In this work, several representative terahertz (THz) graphene holographic impedance surface antenna are presented. Different to the conventional impedance surface antenna that manipulates the surface impedance via varying the patch size in each unit cell, the surface impedance of the proposed antenna in this paper is readily controlled by applying a tunable DC biasing to each graphene patch cell, the physics behind which is that the conductivity of the graphene is a function of imposed voltage. Thus, the graphene patches of the proposed antenna have same size as well as equal spacing, which makes the modeling process more convenient and efficient. Furthermore, for the purpose of beam scanning, the proposed THz graphene holographic antenna can be easily reached by varying the DC supply. Besides, due to the excellent mechanical property of graphene, the proposed THz graphene holographic antenna can be designed conformal to required platforms. To validate and verify the proposed above ideas, a linear polarized with beam scanning capability, a circularized and a conformal THz graphene holographic antenna are designed and simulated via full-wave commercial software HFSS, the simulation results are in good agreements with the design theories.

INDEX TERMS Graphene, holographic antenna, reconfigurability, terahertz (THz).

I. INTRODUCTION

HOLOGRAPHY technology is found by Denis Gabor in optical microscopy in 1948 [1]. Optical holography is a photography technique that uses the principle of interference to record all the information of the object light. It is mainly divided into two parts: hologram recording and object light wave reconstruction. Holographic films are used to record the interference field information of the reference wave and the object light wave, then one can change the reference light through the hologram to obtain the amplitude and phase information of the object light, so the three-dimensional image of the object can be restored. Holographic technology is universal which can be extended to any frequency band as long as there are monochromatic wave sources [2]. Visible light waves and microwaves are both electromagnetic waves in nature and have many identical or similar characteristics, this has led many experts and scholars to expand the application of holographic technology to the microwave frequency region. Inspired by optical principles, Dooley [3] first applied holographic technology to the X-band in 1965, and Kock [4] demonstrated the feasibility of combining holographic principles with antenna technology. Then, a large number of holographic antenna articles were subsequently published [5]–[7].

Around the same time, with the development of artificial electromagnetic material technology, Oliner and Hessel [8] carried out in-depth research on the sinusoidal impedance modulation of metal grating on dielectric substrate, and gave a rigorous derivation. If the modulation period is larger than a certain value, the leaky wave will propagate along the direction away from the surface. According to this principle, a series of leaky wave antennas based on sinusoidal modulated impedance surface are proposed [9]–[11]. On the basis of leaky wave antenna, two-dimensional modulation impedance was realized by Fong *et al.* [12], [13], and they proposed the concept of holographic impedance modulation surface

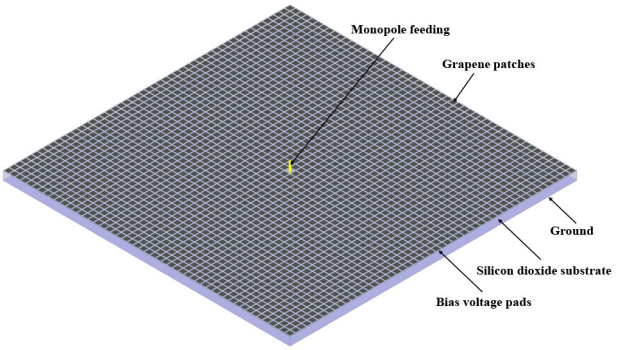

FIGURE 1. The graphene patches on the grounded silicon dioxide dielectric and the polysilicon DC gate pads below form the holographic surface, and it is fed by a monopole in the middle of the surface.

antenna. Using a holographic technique, the interference surface to scatter a known input wave into a desired output wave was designed. The impedance surface consists of a grounded dielectric layer covered with conductive patches. The interference pattern between the current generated by the source and the target field is calculated and designed with metal patches.

Graphene, which is a planar single layer of carbon atoms bonded in a hexagonal structure, has recently triggered extensive attention of the research community due to its unique mechanical, electronic and optical properties characteristics and advantages [14]. Owing to its excellent ability of supporting surface plasmon polariton (SPP) [15] waves [16], and advantages of SPP supported by graphene over plasmon supported by traditional metal materials, a large number of potential applications of graphene SPP [16]–[19] at THz of even optical frequencies have been studied. A particularly promising research field is terahertz and optical wireless communication based on graphene. Nanoscale metallic structures have several drawbacks, including low mobility of electrons and huge channel attenuation, while relatively low loss [20], electronic tunability [21], and strong light-matter interactions [22] are strong points of graphene structures. The unique characteristics of graphene have been used to propose miniaturized and reconfigurable resonance antenna [23]–[25], leaky wave antenna [26]–[29] and reflectarray antenna [30]–[32], which has better radiation efficiency performance than metallic counterparts at THz region, and all of them take full advantage of the reconfigurable characteristics of graphene conductivity [33], [34]. Graphene is regarded as an enabling technology for THz transceivers and optoelectronic systems.

In this paper, several graphene holographic artificial impedance surface antennas in THz region are proposed. By leveraging its conductivity's electric tunable feature, the proposed THz graphene holographic impedance surface antennas can be designed with equally sized and spaced patch cells, and the expected impedance pattern can be conveniently implemented by locally varying the DC biasing for each patch. Also, to achieve beam scanning and polarization conversion, instead of resorting to the traditional geometry revision methodology [12], it only needs to change the DC biasing accordingly. As shown in Fig. 1, the proposed antennas have a general structure which consists of 51×51 equally sized graphene patches. To locally manipulate the conductivity of graphene, a 100nm thick polysilicon DC gate pad is placed below each patch. In addition, its atomic-thickness and outstanding mechanical property make it very suitable for conformal antenna design.

The rest of this paper is organized as follows. In Section III, different types of THz graphene holographic antenna are designed and the related theories are given in detail. Specifically, a linear-polarized holographic antenna with beam scanning capability, a circularly-polarized antenna and a cylindrical conformal antenna are presented. In Section V, conclusions and summaries are given.

II. GRAPHENE PATCH MODELING

A. GRAPHENE CONDUCTIVITY

The atomically-thick graphene can be modulated as an impedance surface with frequency dependent complex conductivity [41] which has both intraband and interband contributions [35], i.e., $\sigma_g(\omega, \mu_c, \Gamma, T) = \sigma' + \mathrm{j}\sigma'' = \sigma_{\text{intra}} + \sigma_{\text{inter}}$. According to the Kubo's formula [36], the conductivity can be formulated as

$$\sigma_g = \frac{jq^2}{\pi\hbar(\omega - j2\Gamma)}\int_0^\infty \varepsilon\left[\frac{\partial f_d(\varepsilon)}{\partial\varepsilon} - \frac{\partial f_d(-\varepsilon)}{\partial\varepsilon}\right]d\varepsilon - \frac{jq^2(\omega - j2\Gamma)}{\pi\hbar^2}\int_0^\infty \frac{f_d(-\varepsilon) - f_d(\varepsilon)}{(\omega - j2\Gamma)^2 - 4(\varepsilon/\hbar)^2}d\varepsilon \quad (1)$$

where ω is the angular frequency, μ_c denotes the chemical potential, $\Gamma = 1/(2\tau)$ is the scattering rate, τ is the relaxation time, T is the temperature, $-q$ is the charge of an electron, $\hbar = h/2\pi$ denotes the reduced Planck's constant, $f_d(\varepsilon) = (e^{(\varepsilon-\mu_c)/k_BT} + 1)^{-1}$ corresponds to the Fermi-Dirac distribution, and k_B denotes the Boltzmann's constant.

The first term in (1) is due to the intraband contributions, and the second term is contributed by the interband conductivity. The intraband contribution is evaluated as

$$\sigma_{\text{intra}} = -\frac{jq^2k_BT}{\pi\hbar^2(\omega - j2\Gamma)}\left[\frac{\mu_c}{k_BT} + 2\ln\left(e^{-\mu_c/k_BT} + 1\right)\right], \quad (2)$$

while the interband contribution can be approximated as

$$\sigma_{\text{inter}} = -\frac{jq^2}{4\pi\hbar}\ln\left[\frac{2|\mu_c| - (\omega - j2\Gamma)\hbar}{2|\mu_c| + (\omega - j2\Gamma)\hbar}\right] \quad (3)$$

for $k_BT \ll |\mu_c|, \hbar\omega$. In this work, only DC supply is applied as the external source while it is free of static magnetic field, thus the conductivity of graphene patch is isotropic [38].

The chemical potential μ_c of the isolated graphene patch is determined by the DC biasing V_{DC} [39], the relationship between them is given by

$$\mu_c \approx \hbar v_F\sqrt{\frac{\pi C_{ox}V_{\text{DC}}}{e}} \quad (4)$$

where $v_F \simeq 9.5\times10^5$m/s [40] means the Fermi velocity, with $C_{\text{ox}} = \varepsilon_r\varepsilon_0/t$ indicating the gate capacitance, $t = 10$nm

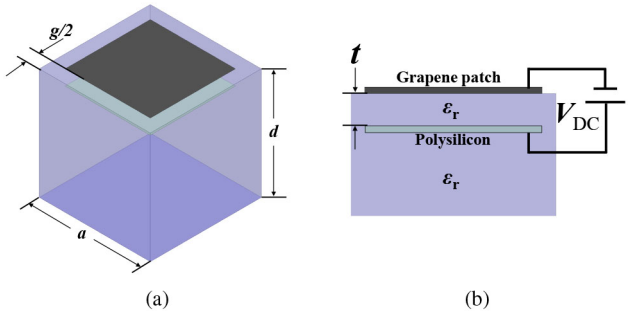

FIGURE 2. Geometrical structure of the unit graphene patch cell, where the gray patch is composed of graphene, and the substrate is silicon dioxide with permittivity ε_r and thickness d, and the thickness of the upper dielectric layer is t (a) Schematic of the unit-cell structure. (b) Cross-section.

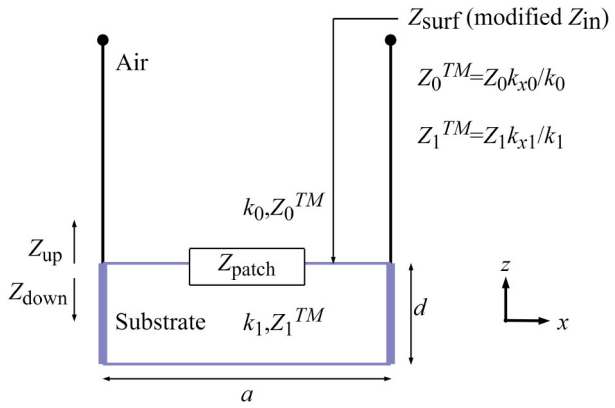

FIGURE 3. The modified transmission line model of TM spp.

is the distance between the biasing pad and graphene patch, and $\varepsilon_r = 4.0$ is the permittivity of the upper silicon dioxide dielectric layer. Thus, the associated conductivity of the graphene can be dynamically controlled via external DC biasing.

In terms of (2) to (4), the desired conductivity can be readily obtained by imposing a proper DC voltage supply. This feature is fully used in this work to create a dynamically controlled artificial impedance surface to radiate different target waves which we will show further detailed next.

B. PATCH IMPEDANCE EXTRACTION

The holographic impedance modulation surface is composed of a number of lattice cells of graphene patches, the structure of the unit cell is shown in Fig. 2, and deposition processes and lithography techniques can be applied to fabrication [26]. Different from the metallic artificial impedance surface, the graphene patches can be arranged in equal dimension for geometry modeling convenience, the target surface impedance can be reached via varying the DC biasing for each patch cell. For the holographic antenna design, the design process mainly involves two aspects: i) the extraction of surface impedance values; ii) the realization of holographic impedance modulation.

Firstly, to realize the target surface impedance pattern determined by the source wave and the target beam, the relationship between the surface impedance and the chemical potential must be established. With this aim in mind, the equivalent circuit model introduced by Patel and Grbic [11] is resorted. It involves calculating the reflection coefficient of the impedance surface, extracting the patch impedance of the graphene layer, and finally calculating the equivalent surface impedance value through the characteristics of the patch impedance and the dielectric layer. The lattice unit can be regarded as a circuit model composed of a graphene patch, a dielectric substrate, and a perfect electrical conductor (PEC) ground plane in parallel. Obviously, the transmission line composed of the substrate are shorted at its ends by the ground plane. According to the transmission line theory, the equivalent parallel can be directly calculated as

$$\frac{1}{Z_{\text{patch}}} = \frac{1}{Z_{\text{in}}} - \frac{1}{jZ_1\tan(k_1 d)} = \frac{1}{Z_{\text{in}}} - \frac{1}{j\frac{Z_0}{\sqrt{\epsilon_r}}\tan\left(k_0\sqrt{\epsilon_r}d\right)}, \tag{5}$$

where the input impedance Z_{in} can be numerically evaluated by applying a vertically incident wave source to illuminate the graphene patch cell. Then, in terms of (5), the equivalent surface impedance value Z_{patch} represented by the patch layer can be obtained.

Since the impedance surface supports the propagation of TM SPP, the patch resistance Z_{patch} cannot be directly used to represent the real impedance, thereby a modified transmission line model [11] shown in Fig. 3 has to be referred. In the modified model, the desired target value Z_{surf} represents the input surface impedance, which is written as Z_{in} in unmodified model. Based on the transverse resonance condition, the relationship between the impedance Z_{down} viewed from above the surface and the impedance Z_{up} viewed from below the surface can be obtained as

$$Z_{\text{up}}(z) + Z_{\text{down}}(z) = 0 \tag{6}$$

Based on (6), this dispersion relation can be reformulated as

$$\frac{1}{Z_{\text{surf}}} = \frac{1}{Z_{\text{patch}}} + \frac{1}{j\frac{Z_0 k_{z1}}{k_0\epsilon_r}\tan(k_{z1}d)} \tag{7}$$

For simplicity but without loss of generality, it is supposed that the ground is located at $z = 0$, it's obvious that $Z_{\text{down}}(z = d^+) = Z_{\text{surf}}$ and $Z_{\text{up}}(z = d^+) = Z_0^{TM}$. Based on the phase matching condition, the phase velocity of the TM wave propagating along the surface should be the same across the air-dielectric interface, namely,

$$k_1^2 - k_{z1}^2 = k_0^2 - k_{x0}^2, \tag{8}$$

then k_{z1} can be obtained as

$$k_{z1} = \sqrt{k_0^2(\epsilon_r - 1) + \left(\frac{Z_{\text{surf}}k_0}{Z_0}\right)^2} \tag{9}$$

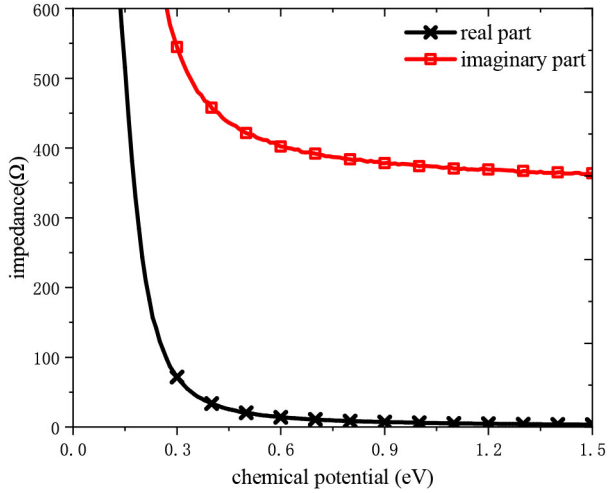

FIGURE 4. Graphene patch surface impedance at 1 THz, the gap between of each patch is g= 7 μm. The range of impedance values affects our choice of parameters X and M.

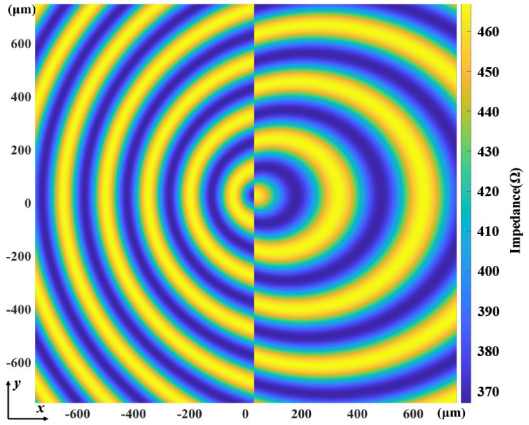

FIGURE 5. The target impedance pattern Z_{surf} when chemical potential varies from 0.4 eV to 1.3 eV, a phase difference equal to π exists on both sides of the y axis to generate TM wave.

By inserting (9) into (7), the surface impedance Z_{surf} can be solved numerically.

To extract the surface impedance for different chemical potential μ_c, the unit cell is simulated with driven-mode simulation in HFSS [42]. The complex conductivity of graphene with thickness of 0.34 nm has been implemented in the simulation using the infinitesimal thin conductive sheet over which a "Impedance" boundary condition is satisfied. For all simulation, the relaxation time of graphene is set to $\tau = 1$ ps and temperature $T = 300$ K, the silicon dioxide is utilized as the substrate with permittivity $\varepsilon_r = 4.0$ and thickness $d = 30$ μm, and the thickness of the upper dielectric layer is 10nm, the lattice constant a and the graphene patch size are set to be 30 μm and 23 μm, respectively, while the chemical potential varies between 0.4 eV and 1.3 eV. In terms of equations above, the calculated surface impedance changes from 33.61+465.24j to 4.22+366.98j, as shown in Fig. 4. By numerical fitting, the analytical relation between the surface impedance Z_{surf} and the chemical potential μ_c is obtained in (10).

$$Z_{\text{surf}} = j\left(343.5 + \frac{29.67}{\mu_c} - \frac{1.851}{\mu_c^2} + \frac{3.308}{\mu_c^3}\right). \tag{10}$$

On the basis of (10) and (4), the desired DC biasing can be quickly obtained once the target impedance Z_{surf} is available.

III. HOLOGRAPHIC PATTERNING

Similar to the optical holography, the surface impedance pattern can be obtained by the interference between the reference and the object wave, which can be expressed as [12]

$$Z(x, y) = j\left[X + M\,\text{Re}\left(\Psi_{\text{obj}}\Psi_{\text{ref}}^*\right)\right], \tag{11}$$

where X is a chosen appropriate reactance mean, M is the modulation depth, Ψ_{obj} represents the target wave, and Ψ_{ref}^* denotes the reference wave. In this work, a short monopole antenna serves as the source antenna, and the generated wave can be approximated as a cylindrical wave, namely,

$$\Psi_{\text{ref}} = e^{-jk_t r} \tag{12}$$

with k_t and r denoting the wave vector of the surface wave and the radial distance between the point on the surface and the monopole, respectively.

The target wave is a plane wave defined as

$$\Psi_{\text{obj}} = e^{jk_0 x \sin\theta + j\phi}, \tag{13}$$

where θ is the radiation direction of target wave. For the convenience of calculation but without affecting the antenna radiation characteristics, the initial phase ϕ is assumed to be 0, and the target radiation beam is propagating in parallel to the X-Z plane.

Since the excited forward and the backward traveling waves along the impedance surface are out of phase, a null depth will be caused at target angle θ. In order to eliminate this singularity point, a load phase modulation technology [37] is deployed to regulate the traveling wave phase. For example, to achieve a vertically polarized wave without null depth, a phase factor equal to π is loaded on the left half region ($x < 0$), the modulation formula is changed from (11) to

$$Z(x, y) = \begin{cases} j\left(X + M\,\text{Re}\left(e^{-jk_0 x \sin\theta} e^{jk_t r}\right), & \text{x} \geq 0 \\ j\left(X + M\,\text{Re}\left(e^{j\pi} e^{-jk_0 x \sin\theta} e^{jk_t r}\right), & \text{x} < 0 \end{cases} \tag{14}$$

In Fig. 5, the target impedance pattern derived in terms of (14) is shown. The corresponding DC biasing for each patch cell can be numerically evaluated according to (4) and (10).

Besides, by further making use of the load phase modulation technology, the circularly polarized beam by merely using scalar holographic impedance surface can also be reached. Since the surface wave of TM mode has in-phase co-polarization and cross-polarization radiation components, a 90° phase shift is introduced to achieve circular polarization characteristics. The rotation direction of circularly polarized

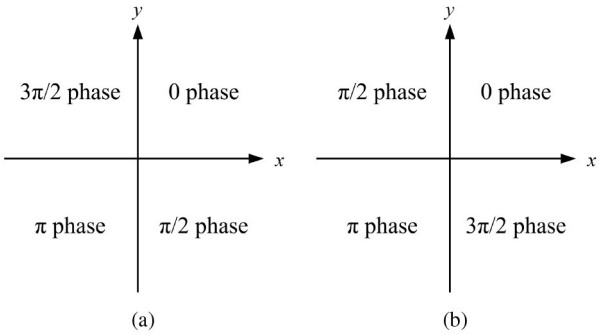

FIGURE 6. Four-phase circular modulation: (a) Four-phase left-hand circular polarization. (b) Four-phase right-hand circular polarization.

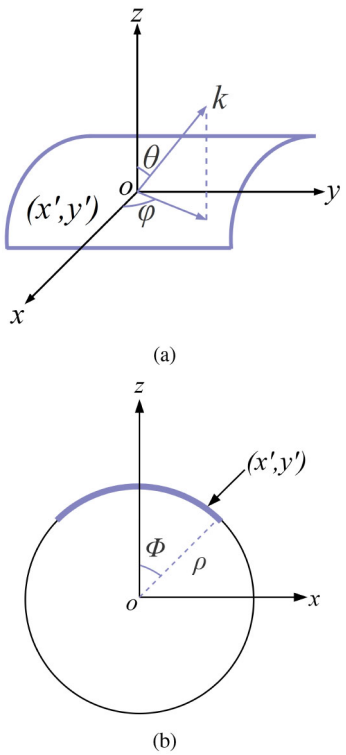

FIGURE 7. Conformal artificial impedance surface: (a) Three-dimensional structure, (b) Side view, the (x',y') is the point coordinate before conformal.

waves is determined by the way in which 90° phase shift is introduced into the impedance surface, as shown in Fig. 6.

Finally, the atomic-thickness and excellent mechanical property of graphene enable the impedance surface to be easily conformal to non-flat surfaces. By coordinate transformation, the target impedance Z_{surf} pertinent to the curve surface can be obtained analytically. For instance, in this work, a holographic antenna structure conformal to a cylinder is presented. The structure of the conformal surface is shown in Fig. 7, and the corresponding impedance Z_{surf} is reformulated as

$$Z(x', y') = j\Big(X + M\,\mathrm{Re}\big(\exp\big(-j\big(k_0\rho\sin\big(x'/\rho\big)\sin\theta + k_0\big(\rho\cos\big(x'/\rho\big) - \rho\big)\cos\theta\big)\big)e^{jk_t r}\Big)\Big) \quad (15)$$

where ρ is the radius of the cylinder, and the (x', y') is the point coordinate of the planar holographic impedance surface before conformal.

IV. DESIGN EXAMPLE

For all examples, a monopole with length equal to 74 μm is employed as the excitation, the substrate is silicon dioxide with permittivity $\varepsilon_r = 4.0$ and thickness $d = 30$ μm. All graphene patches are square patches with length equal to 23 μm, and the neighboring patch cells are equally spaced with pitch size equal to 7 μm, and all antennas operates around 1 THz. The simulation results are given by full-wave commercial software HFSS 2021 [42].

A. A LINEARLY-POLARIZED THZ GRAPHENE HOLOGRAPHIC ANTENNA WITH BEAM SCANNING CAPABILITY

For the first example, a THz holographic antenna with linear polarization is designed. To maximize the modulation capability, the mean reactance and the modulation depth are chosen as $X = 417$ and $M = 50$, respectively, the resultant surface impedance pattern is given as

$$Z_{\text{surf}}(x_t) = \begin{cases} j[417 + 50\cos(k_0 x\sin\theta - k_t r)], & x \geq 0 \\ j[417 - 50\cos(k_0 x\sin\theta - k_t r)], & x < 0 \end{cases} \quad (16)$$

The beam direction θ can be dynamically controlled by varying the chemical potential μ_c of each graphene patch, where the exact value of μ_c is further determined by the DC biasing according to (4) and (10).

In this example, the target beam direction θ of the holographic antenna is designed to point at −30°, 30°, 45°, and 60° in the X-Z plane, respectively. In Fig. 8, the simulated radiation patterns and the required chemical potential of each patch are presented. As can be seen, the practical beam direction is −30°, 30°, 44°, and 57°, respectively, a small shift happening at $\theta = 45°$ and 60° is observed, which can be remedied by slightly modifying the impedance modulation formula without cost. It is also noted that the pertinent gains are 9.24 dB, 9.93 dB, 8.22 dB, and 6.78 dB, respectively, and the corresponding 3 dB beamwidth is 13.89°, 11.25°, 15.46°, and 16.07°, respectively. The bias voltage controlled chemical potential patterns applied to the graphene patches are placed next to the corresponding radiation patterns, and their differences can be easily observed. The practical directivity and the gain of the designed holographic antenna are in good consistent with the expectation.

B. A CIRCULARLY-POLARIZED THZ GRAPHENE HOLOGRAPHIC ANTENNA

As the second example, a THz graphene holographic antenna with circular polarization property is studied. By modifying the loading phase modulation in four quadrants, a $\pi/2$ phase is sequentially added to the four quadrants in a clockwise or a counterclockwise direction, which will lead to a left-hand or a right-hand circularly polarized (LHCP/RHCP) waves accordingly.

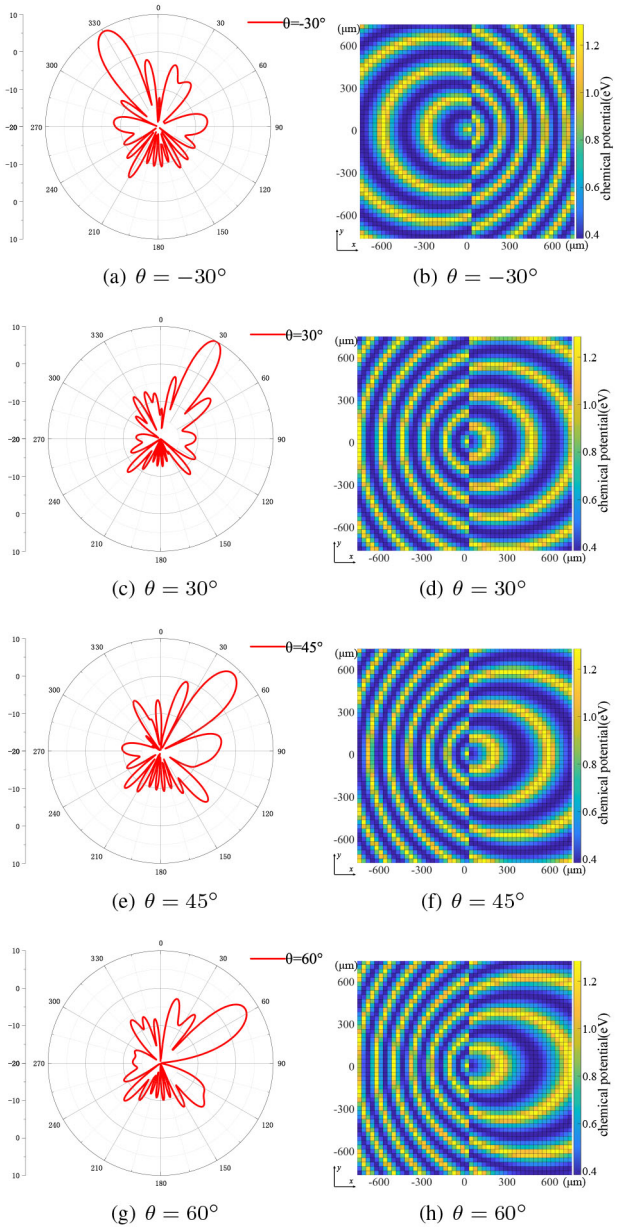

(a) $\theta = -30°$ (b) $\theta = -30°$
(c) $\theta = 30°$ (d) $\theta = 30°$
(e) $\theta = 45°$ (f) $\theta = 45°$
(g) $\theta = 60°$ (h) $\theta = 60°$

FIGURE 8. Radiation patterns and the corresponding required chemical potential changed by the DC biasing of each graphene patch cell for the antenna with different radiation angels, the simulation result of the main beam: (a) 9.24 dB at $\theta = -30°$. (c) 9.93 dB at $\theta = 30°$. (e) 8.22 dB at $\theta = 44°$. (g) 6.78 dB at $\theta = 57°$.

For this example, the beam direction θ of the designed circularly-polarized antenna is set as 30°. Their radiation patterns are shown in Fig. 9(a) and Fig. 9(b) respectively. It can be seen from Fig. 9(a) that the antenna has an obvious main beam in the direction of $\theta = 30°$ in the X-Z plane, with a maximum gain of 9.75 dB, which mainly radiates a LHCP beam. And it can be seen from Fig. 9(b) that the antenna has an obvious main beam in the direction of $\theta = 30°$ in the X-Z plane, and the maximum gain is 9.36 dB, which mainly radiates RHCP beams. The curve of the axial ratio of the antenna changing with the angle θ is shown in the Fig. 10, the 3 dB axial ratio beam angle of the LHCP antenna

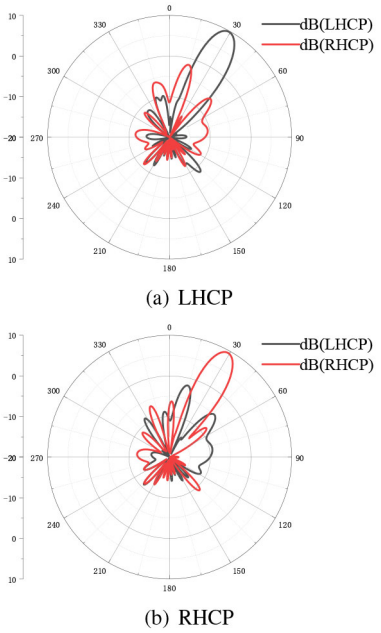

(a) LHCP
(b) RHCP

FIGURE 9. The antenna simulation radiation pattern on the X-Z plane: (a) Left-hand circular polarization; (b) Right-hand circular polarization, the other polarization mode is suppressed.

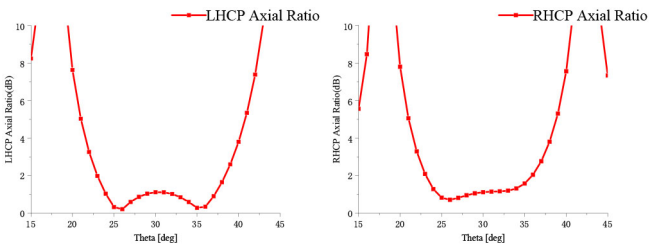

(a) LHCP (b) RHCP

FIGURE 10. The antenna's axial ratio: (a) Left-hand circular polarization. (b) Right-hand circular polarization.

ranges from 22.13° to 39.32°. The 3 dB axial ratio beam angle of the right-hand circularly polarized antenna ranges from 22.17° to 37.21°.

C. A CYLINDRICAL CONFORMAL THZ GRAPHENE HOLOGRAPHIC ANTENNA

In the last example, a THz graphene holographic antenna conformal to a cylindrical surface is benchmaked, as shown in Fig. 11(a). The radius of the cylinder is $\rho = 1530$ μm, and the beam direction is tailored at $\theta = 30°$. On the basis of (15), the desired impedance pattern for this conformal antenna can be easily constructed, where the required chemical potential for each graphene patch cell is shown in Fig. 12.

In Fig. 11(b), the simulated far-field radiation pattern of this conformal antenna in the $\phi = 0°$ plane is shown. It can be seen that the maximum gain of the antenna is around 6.01 dB, the side lobe level is about −3.7 dB, and the front to back ratio is about 14.86 dB. Also, the simulated main beam direction agrees perfectly with the desired one.

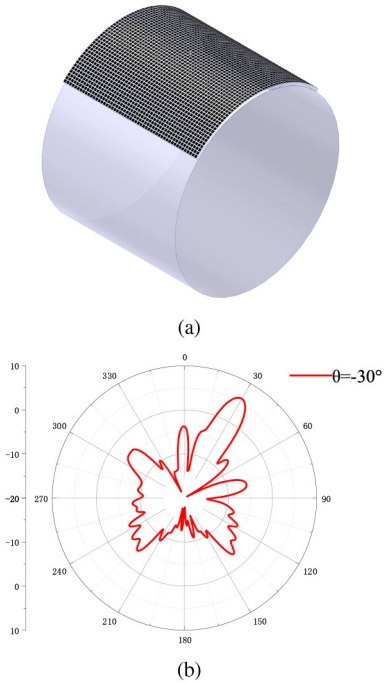

FIGURE 11. Conformal graphene impedance surface: (a) The structure of the conformal antenna. (b) Radiation pattern of conformal surface, the main beam points to 30° and the gain is 6.01dB.

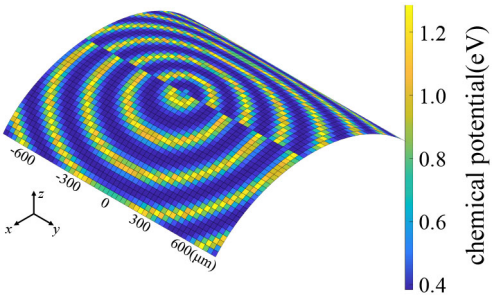

FIGURE 12. Required chemical potential changed by DC biasing of each graphene patch cell for the conformal antenna.

In addition, to study the influence of dimension of the cylinder on the performance of this antenna, the radiation feature of the antenna placed over a cylinder with different radius is simulated. It is found that the larger the radius of the cylinder is, the better performance of the conformal antenna is, such as the higher gain and the lower side lobe level. Because the side of the cylinder with a larger radius is closer to the plane.

V. CONCLUSION

In this work, by using the property of graphene that its conductivity can be dynamically tuned by external DC biasing, several representative terahertz holographic artificial impedance surface antennas are designed and discussed. It is shown that the graphene is very suitable for tunable antenna design, as well as conformal antennas. Its reconfigurable feature makes it a good candidate in future terahertz wireless applications based on graphene. Moreover, the overall high performance of this regular antenna patches array structure is very promising for design and integration of terahertz communication transceivers, sensors and other devices.

REFERENCES

[1] D. Gabor, "A new microscopic principle," *Nature*, vol. 161, pp. 777–778, May 1948, doi: 10.1038/161777a0.
[2] P. Checcacci, V. Russo, and A. Scheggi, "Holographic antennas," *IEEE Trans. Antennas Propag.*, vol. TAP-18, no. 6, pp. 811–813, Nov. 1970, doi: 10.1109/TAP.1970.1139788.
[3] R. P. Dooley, "X-band holography," *Proc. IEEE*, vol. 53, no. 11, pp. 1733–1735, Nov. 1965, doi: 10.1109/PROC.1965.4350.
[4] W. Kock, "Microwave holography," *Microwaves*, vol. 7, pp. 46–54, Nov. 1968.
[5] P. Checcacci, G. Papi, and V. Russo, "A holographic VHF antenna," *IEEE Trans. Antennas Propag.*, vol. TAP-19, no. 2, pp. 278–279, Mar. 1971, doi: 10.1109/TAP.1971.1139915.
[6] J. Bennett, A. Anderson, P. McInnes, and A. Whitaker, "Microwave holographic metrology of large reflector antennas," *IEEE Trans. Antennas Propag.*, vol. TAP-24, no. 3, pp. 295–303, May 1976, doi: 10.1109/TAP.1976.1141354.
[7] K. Iizuka, M. Mizusawa, S. Urasaki, and H. Ushigome, "Volume-type holographic antenna," *IEEE Trans. Antennas Propag.*, vol. TAP-23, no. 6, pp. 807–810, Nov. 1975, doi: 10.1109/TAP.1975.1141175.
[8] A. Oliner and A. Hessel, "Guided waves on sinusoidally-modulated reactance surfaces," *IEEE Trans. Antennas Propag.*, vol. TAP-7, no. 5, pp. 201–208, Dec. 1959, doi: 10.1109/TAP.1959.1144771.
[9] F. Caminita, M. Nannetti, and S. Maci, "A design method for curvilinear strip grating holographic antennas," in *Proc. Antennas Propag. Soc. Int. Symp.*, San Diego, CA, USA, 2008, pp. 1–4.
[10] F. Caminita, M. Nannetti, and S. Maci, "Holographic surfaces realized by curvilinear strip gratings," in *Proc. 2nd Eur. Conf. Antennas Propag. (EuCAP)*, Nov. 2007, pp. 1–4.
[11] A. M. Patel and A. Grbic, "A printed leaky-wave antenna based on a sinusoidally-modulated reactance surface," *IEEE Trans. Antennas Propag.*, vol. 59, no. 6, pp. 2087–2096, Jun. 2011, doi: 10.1109/TAP.2011.2143668.
[12] B. H. Fong, J. S. Colburn, J. J. Ottusch, J. L. Visher, and D. F. Sievenpiper, "Scalar and tensor holographic artificial impedance surfaces," *IEEE Trans. Antennas Propag.*, vol. 58, no. 10, pp. 3212–3221, Oct. 2010, doi: 10.1109/TAP.2010.2055812.
[13] B. H. Fong, J. S. Colburn, P. R. Herz, J. J. Ottusch, D. F. Sievenpiper, and J. L. Visher, "Polarization controlling holographic artificial impedance surfaces," in *Proc. IEEE Antennas Propag. Soc. Int. Symp.*, Honolulu, HI, USA, Jun. 2007, pp. 3824–3827.
[14] A. K. Geim and K. S. Novoselov, "The rise of graphene," *Nat. Mater.*, vol. 6, pp. 183–191, Mar. 2007, doi: 10.1038/nmat1849.
[15] J. M. Pitarke, V. M. Silkin, E. V. Chulkov, and P. M. Echenique, "Theory of surface plasmons and surface-plasmon polaritons," *Rep. Progr. Phys.*, vol. 70, no. 1, pp. 1–87, Dec. 2006, doi: 10.1088/0034-4885/70/1/r01.
[16] A. Vakil and N. Engheta, "Transformation optics using graphene," *Science*, vol. 332, no. 6035, pp. 1291–1294, Jun. 2011, doi: 10.1126/science.1202691.
[17] A. N. Grigorenko, M. Polini, and K. S. Novoselov, "Graphene plasmonics," *Nat. Photon.*, vol. 6, no. 11, pp. 749–758, Nov. 2012, doi: 10.1038/nphoton.2012.262.
[18] J. S. Gómez-Díaz and J. Perruisseau-Carrier, "Graphene-based plasmonic switches at near infrared frequencies," *Opt. Exp.*, vol. 21, no. 13, pp. 15490–15504, Jul. 2013, doi: 10.1364/OE.21.015490.
[19] M. Jablan, H. Buljan, M. Soljačić, "Plasmonics in graphene at infrared frequencies," *Phys. Rev. B, Condens. Matter*, vol. 80, no. 24, Dec. 2009, Art. no. 245435, doi: 10.1103/PhysRevB.80.245435.
[20] J. Christensen, A. Manjavacas, S. Thongrattanasiri, F. H. L. Koppens, and F. J. G. de Abajo, "Graphene plasmon waveguiding and hybridization in individual and paired nanoribbons," *ACS Nano*, vol. 6, no. 1, pp. 431–440, 2012, doi: 10.1021/nn2037626.
[21] K. S. Novoselov *et al.*, "Electric field effect in atomically thin carbon films," *Science*, vol. 306, no. 5696, pp. 666–669, Oct. 2004, doi: 10.1126/science.1102896.
[22] F. H. L. Koppens, D. E. Chang, and F. J. G. de Abajo, "Graphene plasmonics: A platform for strong light–matter interactions," *Nano Lett.*, vol. 11, no. 8, pp. 3370–3377, Aug. 2011, doi: 10.1021/nl201771h.

[23] M. Tamagnone, J. S. Gomez-Diaz, J. R. Mosig, and J. Perruisseau-Carrier, "Reconfigurable terahertz plasmonic antenna concept using a graphene stack," *Appl. Phys. Lett.*, vol. 101, no. 21, Oct. 2012, Art. no. 214102, doi: 10.1063/1.4767338.

[24] I. Llatser, C. Kremers, A. Cabellos-Aparicio, J. M. Jornet, E. Alarcón, and D. N. Chigrin, "Graphene-based nano-patch antenna for terahertz radiation," *Photon. Nanostruct. Fundam. Appl.*, vol. 10, no. 4, pp. 353–358, Oct. 2012, doi: 10.1016/j.photonics.2012.05.011.

[25] D. Correas-Serrano, J. S. Gomez-Diaz, A. Alù, and A. Álvarez-Melcón, "Electrically and magnetically biased graphene-based cylindrical waveguides: Analysis and applications as reconfigurable antennas," *IEEE Trans. THz Sci. Technol.*, vol. 5, no. 6, pp. 951–960, Nov. 2015, doi: 10.1109/TTHZ.2015.2472985.

[26] M. Esquius-Morote, J. S. Gómez-Díaz, and J. Perruisseau-Carrier, "Sinusoidally modulated graphene leaky-wave antenna for electronic beamscanning at THz," *IEEE Trans. THz Sci. Technol.*, vol. 4, no. 1, pp. 116–122, Jan. 2014, doi: 10.1109/TTHZ.2013.2294538.

[27] D. A. Chu, P. W. C. Hon, T. Itoh, and B. S. Williams, "Feasibility of graphene CRLH metamaterial waveguides and leaky wave antennas," *J. Appl. Phys.*, vol. 120, no. 1, Jul. 2016, Art. no. 13103, doi: 10.1063/1.4955138.

[28] P.-Y. Chen, M. Farhat, A. N. Askarpour, M. Tymchenko, and A. Alú, "Infrared beam-steering using acoustically modulated surface plasmons over a graphene monolayer," *J. Opt.*, vol. 16, no. 9, Sep. 2014, Art. no. 94008, doi: 10.1088/2040-8978/16/9/094008.

[29] D. Correas-Serrano, J. S. Gomez-Diaz, D. L. Sounas, Y. Hadad, A. Alvarez-Melcon, and A. Alú, "Nonreciprocal graphene devices and antennas based on spatiotemporal modulation," *IEEE Antennas Wireless Propag. Lett.*, vol. 15, pp. 1529–1533, 2016, doi: 10.1109/LAWP.2015.2510818.

[30] E. Carrasco, M. Tamagnone, J. R. Mosig, T. Low, and J. Perruisseau-Carrier, "Gate-controlled mid-infrared light bending with aperiodic graphene nanoribbons array," *Nanotechnology*, vol. 26, no. 13, Mar. 2015, Art. no. 134002, doi: 10.1088/0957-4484/26/13/134002.

[31] E. Carrasco, M. Tamagnone, and J. Perruisseau-Carrier, "Tunable graphene reflective cells for THz reflectarrays and generalized law of reflection," *Appl. Phys. Lett.*, vol. 102, no. 10, pp. 1–5, 2013, doi: 10.1063/1.4795787.

[32] E. Carrasco and J. Perruisseau-Carrier, "Reflectarray antenna at terahertz using graphene," *IEEE Antennas Wireless Propag. Lett.*, vol. 12, pp. 253–256, 2013, doi: 10.1109/LAWP.2013.2247557.

[33] J. Perruisseau-Carrier, M. Tamagnone, J. S. Gomez-Diaz, and E. Carrasco, "Graphene antennas: Can integration and reconfigurability compensate for the loss?" in *Proc. Eur. Microw. Conf.*, Nuremberg, Germany, 2013, pp. 369–372.

[34] D. Correas-Serrano and J. S. Gomez-Diaz, "Graphene-based antennas for terahertz systems: A review," 2017, *arXiv:1704.00371*.

[35] S. H. Zainud-Deen, A. M. Mabrouk, and H. A. Malhat, "Frequency tunable graphene metamaterial reflectarray for terahertz applications," *J. Eng.*, vol. 2018, pp. 753–761, Sep. 2018, doi: 10.1049/joe.2018.5016.

[36] G. W. Hanson, "Dyadic green's functions and guided surface waves for a surface conductivity model of graphene," *J. Appl. Phys.*, vol. 103, no. 6, Mar. 2008, Art. no. 64302, doi: 10.1063/1.2891452.

[37] S. Pandi, C. A. Balanis, and C. R. Birtcher, "Design of scalar impedance holographic metasurfaces for antenna beam formation with desired polarization," *IEEE Trans. Antennas Propag.*, vol. 63, no. 7, pp. 3016–3024, Jul. 2015, doi: 10.1109/TAP.2015.2426832.

[38] G. Lovat, "Equivalent circuit for electromagnetic interaction and transmission through graphene sheets," *IEEE Trans. Electromagn. Compat.*, vol. 54, no. 1, pp. 101–109, Feb. 2012, doi: 10.1109/TEMC.2011.2169072.

[39] K. Rouhi, S. E. Hosseininejad, S. Abadal, M. Khalily, and R. Tafazolli, "Multi-channel near-field terahertz communications using reprogrammable graphene-based digital metasurface," *J. Lightw. Technol.*, vol. 39, no. 21, pp. 6893–6907, Nov. 1, 2021, doi: 10.1109/JLT.2021.3105911.

[40] K. R. Knox *et al.*, "Spectromicroscopy of single and multilayer graphene supported by a weakly interacting substrate," *Phys. Rev. B, Condens. Matter*, vol. 78, no. 20, Nov. 2008, Art. no. 201408, doi: 10.1103/physrevb.78.201408.

[41] V. Nayyeri, M. Soleimani, and O. M. Ramahi, "Modeling graphene in the finite-difference time-domain method using a surface boundary condition," *IEEE Trans. Antennas Propag.*, vol. 61, no. 8, pp. 4176–4182, Aug. 2013, doi: 10.1109/TAP.2013.2260517.

[42] Ansoft Corporation. "High Frequency Structure Simulator (HFSS)." Software of HFSS. (Accessed: 2021). [Online]. Available: https://www.ansys.com/products/electronics/ansys-hfss/

PENGFEI REN received the bachelor's degree in information engineering from Shanghai Jiao Tong University, Shanghai, China, in 2020, where he is currently pursuing the master's degree in electronics and communication engineering with the Department of Electronics. His current research interests include terahertz antenna design, filters, leaky wave antenna, spoof surface plasmon polaritons, and computational electromagnetics.

LIJUN JIANG received the B.S. degree in electrical engineering from the Beijing University of Aeronautics and Astronautics, Beijing, China, in 1993, the M.S. degree from Tsinghua University, Beijing, in 1996, and the Ph.D. degree from the University of Illinois at Urbana–Champaign, Champaign, IL, USA, in 2004.

From 1996 to 1999, he was an Application Engineer with Hewlett-Packard Company, Beijing. He was with Semiconductor Research Cooperation Industrial Liaison, Hong Kong, for several academic projects. Since 2004, he has been a Postdoctoral Researcher, a Research Staff Member, and a Senior Engineer with IBM T. J. Watson Research Center, Yorktown Heights, NY, USA. Since 2009, he has been an Associate Professor with the Department of Electrical and Electronic Engineering, The University of Hong Kong, Hong Kong. He served as a Scientific Consultant with Hong Kong Applied Science and Technology Research Institute Company Ltd., Hong Kong, from 2010 to 2011. Since 2013, he has been a Senior Visiting Professor with Tsinghua University. He has been serving as a Panelist on the Expert Review Panel for the Hong Kong Research and Development Center for Logistics and Supply Chain Management Enabling Technologies, Hong Kong, since 2013. He has been involved collaboratively with many international researchers.

Dr. Jiang was a recipient of the IEEE MTT Graduate Fellowship Award in 2003 and the Y. T. Lo Outstanding Research Award in 2004. He was a session chair of many international conferences. He was the TPC Chair of the 7th International Conference on Nanophotonics/the 3rd Conference on Advances in Optoelectronics and Micro/Nano Optics, the TPC Co-Chair of the 12th International Workshop on Finite Elements for Microwave Engineering and the 2013 International Workshop on Pulsed Electromagnetic Field at Delft, The Netherlands, and the General Chair of the 2014 IEEE 14th HK AP/MTT Postgraduate Conference. He was an Associate Guest Editor of the PROCEEDINGS OF THE IEEE special issue from 2011 to 2012. He is an Associate Editor of the IEEE TRANSACTIONS ON ANTENNAS AND PROPAGATION and *Progress in Electromagnetics Research*. He also serves as a Reviewer for the IEEE Transactions on Several Topics and Other Primary Electromagnetics and Microwave-Related Journals. He has been an Elected TPC Member of the IEEE Electrical Design of Advanced Packaging and Systems Symposium (EDAPS) since 2010 and the IEEE Electrical Performance of Electronic Packaging since 2014. He was a TPC Member of the 2013 IEEE International Conference on Microwave Technology and Computational Electromagnetics. He has been a TC-9 Member and a TC-10 Member of the IEEE Electromagnetic Compatibility Society since 2011. He was a Scientific Committee Member of the 2010 IEEE Simulation and Modeling of Emerging Electronics, the Special Session Organizer of the IEEE EDAPS, the IEEE Electromagnetic Compatibility, Applied Computational Electromagnetics Society, Asia–Pacific Radio Science Conference, Progress in Electromagnetics Research Symposium, and a Co-Organizer of the HKU Computational Science and Engineering Workshops from 2010 to 2012. He is a member of the IEEE Antennas and Propagation Society, the IEEE Microwave Theory and Techniques Society, the IEEE Electromagnetic Compatibility Society, the ACES, and the Chinese Computational Electromagnetics Society.

PING LI (Senior Member, IEEE) received the B.S. degree in physical electronics engineering and the master's degree from the University of Electronic Science and Technology of China, Chengdu, China, in 2008 and 2010, respectively, and the Ph.D. degree in electrical and electronic engineering from The University of Hong Kong (HKU), Hong Kong, in 2014.

From October 2014 to December 2015, he was a Postdoctoral Fellow with the Computational Electromagnetics Laboratory, King Abdullah University of Science and Technology (KAUST), Thuwal, Saudi Arabia. From December 2015 to December 2016, he was a Postdoctoral Fellow with the On-Chip Electromagnetics Laboratory, Purdue University, West Lafayette, IN, USA. From January 2017 to August 2018, he joined the Department of Electrical and Electronic Engineering, HKU, as a Research Assistant Professor. From September 2018 to August 2019, he was a Research Scientist with KAUST, as well as a Honorary Assistant Professor, HKU. Since August 2019, he has been joined Shanghai Jiao Tong University as an Associate Professor.

Dr. Li was a recipient of the 2018 Joint IEEE EMC and APEMC Outstanding Young Scientist Award, the 2018 ACES-China Young Scientist Award, the 40th PIERS Young Scientist Award in Japan, and the Okawa Research Foundation Grant of Japan. Besides, he was a recipient of the 2018 Best Annual Paper Prize on *Chinese Journal of Radio Science*, and a recipient of the Second Prize Award for Natural Sciences of Chinese Institute of Electronics, 2019. Besides, his paper was selected as the Finalist paper in 29th International Review of Progress in Applied Computational Electromagnetics and 2014 International Symposium on Electromagnetic Compatibility, and he won the Best Student Paper Award in 12th International Workshop on Finite Elements for Microwave Engineering.